



Identification of PDE4B Over 4D subtype-selective inhibitors revealing an unprecedented binding mode

Michael Kranz *, Michael Wall, Brian Evans, Afjal Miah, Stuart Ballantine, Chris Delves, Brian Dombroski, Jeffrey Gross, Jessica Schneck, James P. Villa, Margarete Neu, Don O. Somers

Medicines Research Centre, GlaxoSmithKline, Gunnels Wood Road, Stevenage, Hertfordshire, SG1 2NY, England, UK

ARTICLE INFO

Article history:

Received 27 November 2008
Revised 27 March 2009
Accepted 31 March 2009
Available online 5 April 2009

Keywords:

Lead optimisation
Ligand docking
Induced fit
SAR

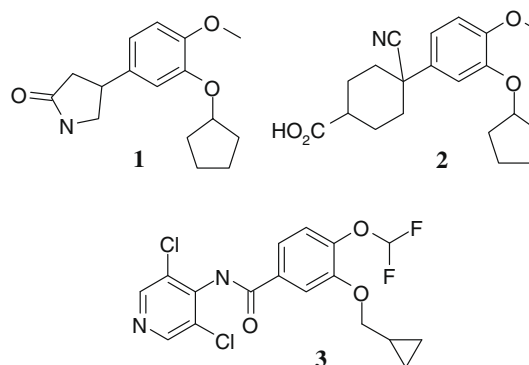
ABSTRACT

A PDE4B over 4D-selective inhibitor programme was initiated to capitalise on the recently discovered predominance of the PDE4B subtype in inflammatory cell regulation. The SAR of a tetrahydrobenzothio-*phene* (THBT) series did not agree with either of two proposed docking modes in the 4B binding site. A subsequent X-ray co-crystal structure determination revealed that the THBT ligand displaces the Gln-443 residue, invariably ligand-anchoring in previous PDE4 co-crystal structures, and even shifts helix-15 by 1–2 Å. For the first time, several residues of the C-terminus previously proposed to be involved in subtype selectivity are resolved and three of them extend into the ligand binding site potentially allowing for selective drug design.

© 2009 Elsevier Ltd. All rights reserved.

1. Introduction

For exactly 4 decades, inhibitors of 3',5'-nucleotide phosphodiesterase enzymes (PDE) have been known.¹ The initially discovered natural product inhibitors, like papaverine, were found to interfere with the hydrolysis of the endogenous substrates of cAMP and cGMP non-selectively for the various PDE subtypes. The dominant therapeutic role of the PDE4 protein family was established through the action of the first-generation PDE4 inhibitor rolipram **1** as an antidepressant agent.² The dose-limiting side effects of nausea and vomiting were reduced by second-generation inhibitors like cilomilast (Ariflo, **2**) and roflumilast **3**, which have succeeded as anti-inflammatories in clinical trials for COPD and asthma as oral agents, but their therapeutic index has prevented market launch so far.³ Most recent studies have linked the PDE4B subtype to inflammatory cell regulation⁴ while the PDE4D subtype is implied in the emetic response.⁵ Consequently, this paper describes how we tried to optimise the potency of a PDE4B-selective hit from an HTS based on docking models. The X-ray structure of a lead molecule surprised with an unexpected binding mode and an unprecedented active site deformation.



2. Results and discussion

2.1. Initial docking mode

During an HTS campaign, a tetrahydrobenzothio-*phene* (THBT) bisamide (**4**) was discovered to be a potent and modestly PDE4B-over 4D-selective inhibitor (PDE3 (bovine enzyme SPA assay) and PDE5 (human enzyme SPA assay) had a $pIC_{50} < 5$). With a large number of in-house and published ligand/PDE4B catalytic domain co-crystal structures available,⁶ it was hoped that elucidation of the THBT binding mode would drive the analogue selection to derive PDE4B- over 4D-selective SAR.⁷

* Corresponding author. Tel.: +44 1438 763385; fax: +44 1438 763352.
E-mail address: michael.j.kranz@gsk.com (M. Kranz).

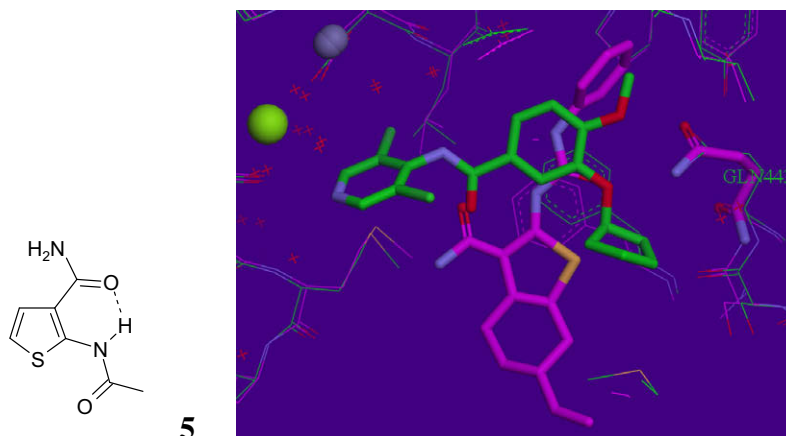
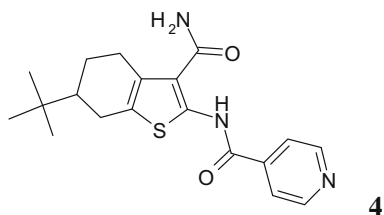


Figure 1. Preferred conformation of the thiophene bisamide and the 2-amide-anchored docking mode (Flo+) of a THBT (magenta) overlaid with the X-ray of piclamilast (1xm4; green).



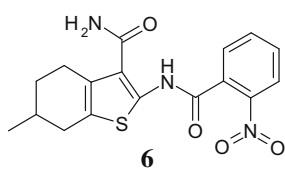
PDE4B/4D pIC₅₀⁷ 6.7/6.5

A search in the CDC database⁸ confirmed the assumption that the bisamide system is fixed through an intramolecular H bond (5 in Fig 1). It is known that the prerequisite for PDE4 activity is a flat aromatic system fitting into the 'hydrophobic clamp' as well as an H bond acceptor for the Gln-443 amino group.⁹ With the amide conformations fixed as described above, both carbonyl oxygens as well as the sulfur (although a very weak H bond acceptor)¹⁰ were individually coordinated to the ligand-anchoring Gln-443 while keeping the template ring system in the 'hydrophobic clamp' of the PDE4 catalytic site.

After optimisation of the ligand position (Flo+, ThistleSoft),¹¹ the sulfur or the 3-amide carbonyl coordination to Gln-443 would lead to serious clashes in the deep end of the enzyme pocket whereas the 2-amide carbonyl gives a reasonable docking fit for this template (Fig. 1). In this pose, the aryl ring occupies the same small pocket as the methoxy group of piclamilast (1xm4),¹² the primary amide points into the water-filled part of the binding site while the tetrahydrobenzo group orientates to the pocket exit suggesting ample scope for substitution at both positions.

2.2. Chemistry

A substructure search of in-house thiophene bisamides resulted in 32 compounds fitting the initial docking model. The most active hit 6 demonstrated significant (10-fold) selectivity against the 4D subtype and represented a suitable starting point from which to launch our hit-to-lead effort.

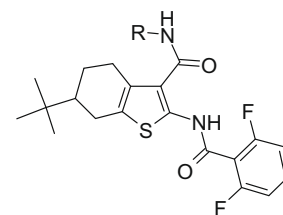


PDE4B/4D pIC₅₀ 7.3/6.3

An initial array was undertaken to probe the proposed binding mode. Key compounds were synthesised according to the general pathway described in Scheme 1. The intermediate ethyl 2-amino-4,5,6,7-tetrahydro-1-benzothiophene-3-carboxylate 8 and 2-amino-4,5,6,7-tetrahydro-1-benzothiophene-3-carboxamide 11 were prepared using known reaction conditions¹³ using a suitably substituted cycloketone in a one pot procedure and in good yields. It was demonstrated that functionality could be built into the THBT scaffold at this stage whereby ketones with a variety of substitution patterns R¹ = (alkyl, aryl, protected amine, protected ketone, CH₂) R² = (alkyl, CH₂) R³ = (Alkyl, CH₂) were used to synthesise the corresponding thiophenes. Regioisomers were separable in some cases at this stage, however where necessary only, it was decided to separate these at the final stage in the synthesis.

Diversity at the 3-carboxy position was introduced through amide coupling. Saponification of the ethyl ester 8 using sodium hydroxide gave the carboxylic acid. Subsequent treatment of the acid using HATU as the coupling agent and the appropriate amine gave compounds of type 9 in good yields. Alternatively, the primary carboxamide 11 could be accessed in a one pot procedure using the conditions of cyclisation described above.

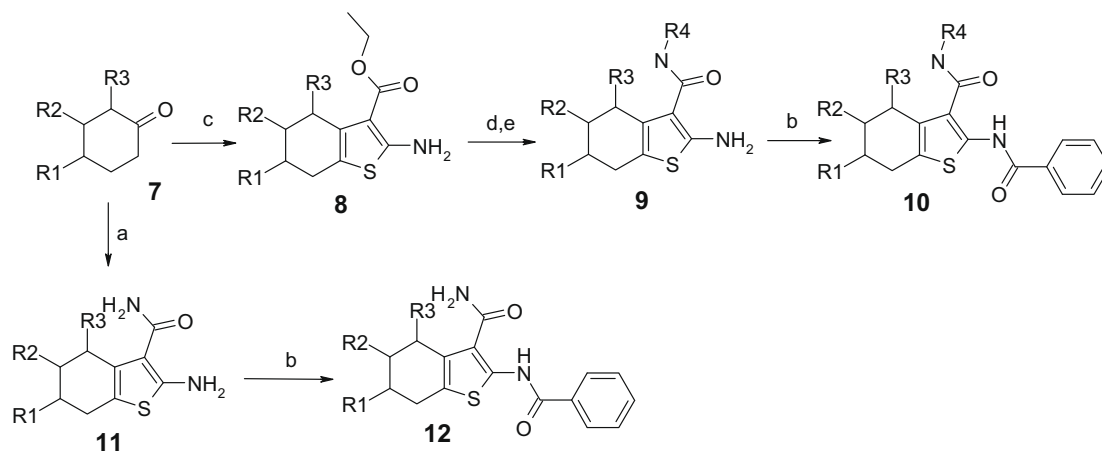
Optimal conditions for acylation at the 2-amino thiophene were found when the reaction was carried out in pyridine in the presence of the corresponding acyl chlorides or fluorides, either pre-formed or generated in situ and furnished the final compounds of types 11 and 12.



PDE4B pIC₅₀ R = H (13a): 7.1; R = Me (13b): < 5

2.3. Alternative binding mode

Initial SAR at the 3-carboxy position showed significantly reduced potencies when the primary amide was methylated as exemplified by 13a/b and indicated a clear requirement for the primary carboxamide at this position. This suggested that the current docking hypothesis was untenable as the primary carboxamide



Scheme 1. Reagents and conditions: (a) 2-cyanoacetamide, sulfur, morpholine, ethanol, 80 °C 80–95%. (b) Acid chloride, pyridine, 25 °C 65–95%. (c) Ethyl cyanoacetate, sulfur, morpholine, ethanol, 80 °C, 80–95%. (d) (i) NaOH, methanol/water (1:1), 100 °C, (ii) H⁺. (e) HATU, Amine, *i*-Pr₂NEt, DMF, 25 °C. R1, R2, R3 can be 2H, alkyl or aryl, protected amine or ketone and R4 can be H, alkyl or aryl.

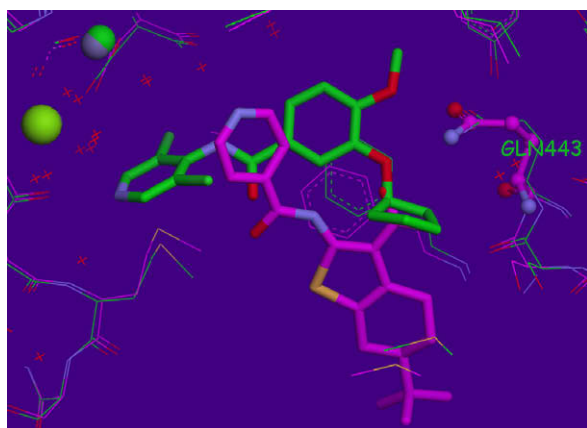
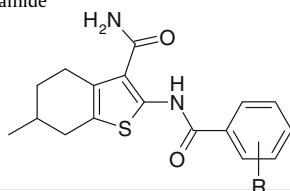


Figure 2. Overlay of the X-ray of piclamilast in PDE4B (1xm4; green) and the second lowest energy docking pose for the alternative amide anchoring of a THBT (magenta).

Table 1
SAR around the phenylamide

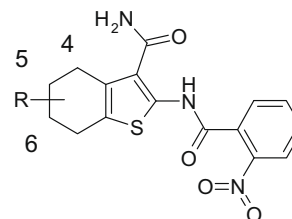


| R | <i>p</i> IC ₅₀ PDE4B | <i>p</i> IC ₅₀ PDE4D |
|---|---------------------------------|---------------------------------|
| <i>o</i> -NO ₂ (6) | 7.3 | 6.3 |
| <i>m</i> -NO ₂ (14) | 6.2 | <5.6 |
| <i>p</i> -NO ₂ (15) | <5.6 | <5.6 |

herein points into a water-filled pocket that should disfavour a methylated amide but should not render the molecule completely inactive.

To give credit to the significance of the primary amide, this group was coordinated to Gln-443 and a conformational search was performed in the binding site (Flo+). The lowest energy structure also had the pyridyl ring in a similar vicinity to the piclamilast methoxy group as shown in the overlay in Figure 1. The second lowest binding mode has the ligand less deeply buried in the pocket thus bringing the thiophene ring system closer to the binding

Table 2
SAR around the tetrahydrobenzo group



| R | <i>p</i> IC ₅₀ PDE4B | <i>p</i> IC ₅₀ PDE4D |
|-------------------------------------|---------------------------------|---------------------------------|
| H (16) | 5.9 | 5.2 |
| 4-Me (17) | 5.3 | 4.5 |
| 4-(2,6-Toluy) (18) | 5.3 | 5.6 |
| 5-Me (19) | 5.7 | 5.2 |
| 5- <i>t</i> Bu (20) | 5.9 | 5.2 |
| 6-Me (6) | 7.3 | 6.3 |
| 6-Et (21) | 8.0 | 6.9 |
| 6- <i>t</i> Bu (22) | 7.6 | 6.9 |
| 6,6-(Me) ₂ (23) | 7.3 | 6.4 |
| 6- <i>n</i> -Pn (24) | 7.0 | 5.6 |
| 6-Ph (25) | 6.4 | 5.8 |

site exit (Fig. 2) where the 4B/4D selectivity is thought to be determined.¹⁴ This model also suggests that there is enough space around the *ortho*- and *meta*-positions of the phenyl ring of **13a** to account for the observed SAR, with the *para*-position blocked by the protein, also in agreement with the SAR (Table 1).

The emerging SAR around the tetrahydrobenzo group confirms the 4B-subtype selectivity of this series and indicates a preference for small C6 substituents (Table 2). High potency was achieved where R = 6-ethyl **21**, whilst maintaining the 10-fold selectivity index. However, this feature cannot be reconciled with the alternative binding mode. Throughout the progress of the programme, crystallisation efforts were undertaken to facilitate a structure-based drug design approach.

2.4. Binding mode in co-crystal structure

Constructs previously used in crystallography¹⁵ have focused on the catalytic domain from residue 152 to residues 503, 506 and 528 but resolving a structure beyond about residue 487 has been successful only once.¹⁶ The C-terminal residues 496–508 have been resolved in a PDE4B apo-structure but their provenance

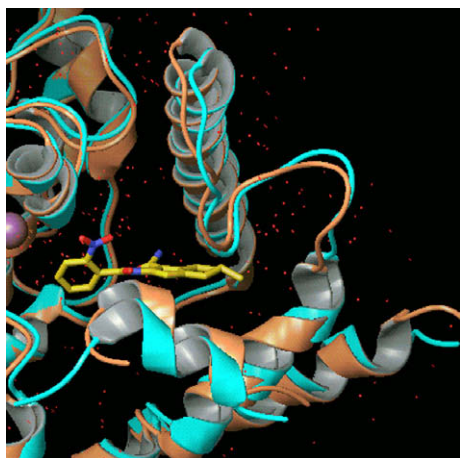


Figure 3. Overlay of PDE4B/THBT ligand complex (cyan) and unliganded 1f0j (1.8 Å resol.; orange) X-rays; helix-14 above ligand, helix-15 to the right, helix-16 far right.

from a neighbouring protein led the authors to describe this interaction as a crystallographic artefact. In addition, some of the side chains extend into the binding pocket preventing any potential ligand binding.

Further crystallisation attempts were made on the longest protein construct (and others generated from extensive cloning and expression studies)¹⁷ based on the hypothesis that the PDE4B/4D

selectivity-determining residues reside within the C-terminus of PDE4 located just outside the catalytic pocket.¹⁴ This effort led to a new crystal form produced from construct PDE4B2 152–528 (triple mutant) co-crystallised with a THBT inhibitor (**13**) that allowed the structure of additional C-terminal residues Asp-498 to Glu-509 to be built and shows the THBT bound in a completely unexpected way.

The THBT ligand binds deep in the binding site, perpendicular to both computationally predicted poses, forcing an unprecedented distortion of several catalytic domain helices (Fig. 3). Most remarkably, the ligand enlarges the catalytic pocket by forcing the top of helix-15 a distance of 1–2 Å outwards together with the termini of helix-14 and -16.

While the ligand still slots into the ‘hydrophobic clamp’, the obligatory H bond to Gln-443 is not only absent but this residue is pushed from its position in all known PDE4 X-ray structures (Fig. 4). The Gln amide plane is almost perpendicular to the usual orientation and the amino group forms an H bond with Thr-407.



Figure 6. C-terminal residues resolved in THBT PDE4B X-ray structure.

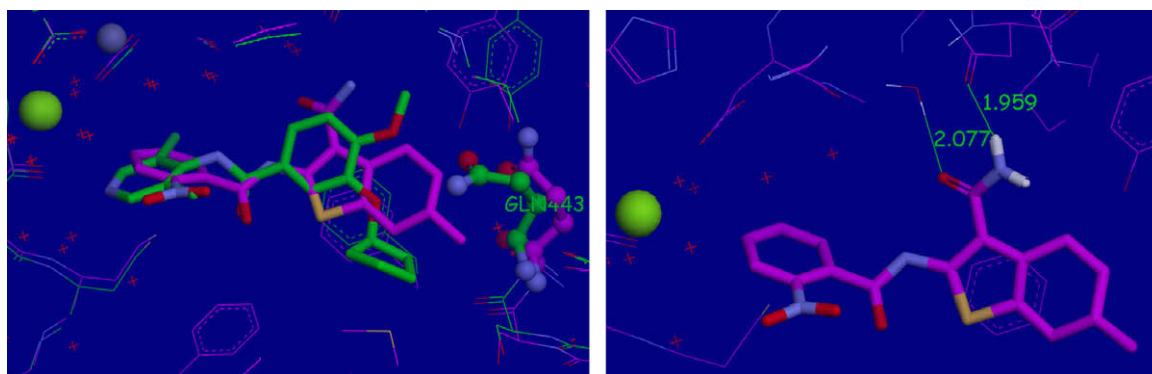


Figure 4. Overlay of the X-rays of piclamilast (green) and THBT **13** (magenta).

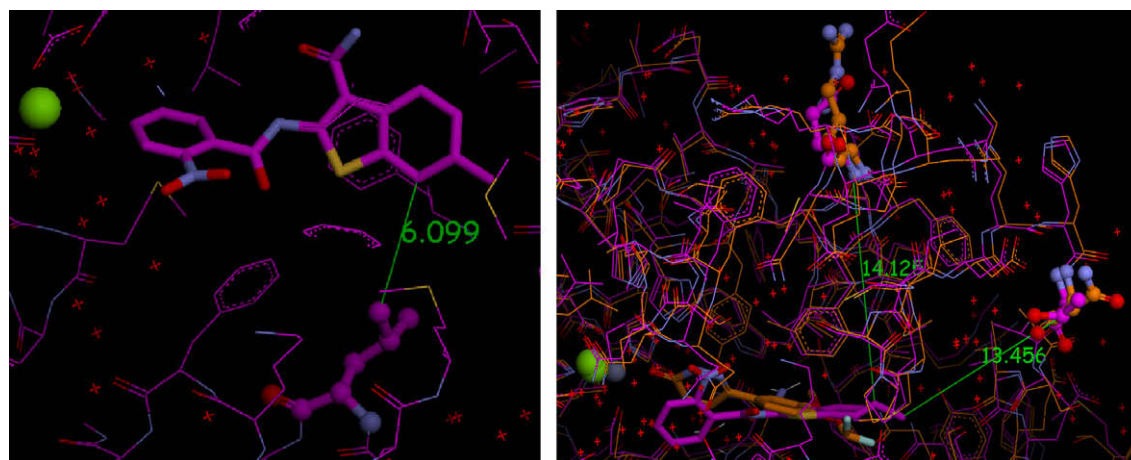


Figure 5. PDE4B/THBT X-ray and overlay of PDE4B/THBT (magenta) and PDE4D/zardaverine (1xor, 1.5 Å resol.; orange) X-rays and shortest distance of ligand to the 2 closest 4B/4D side chain variations.

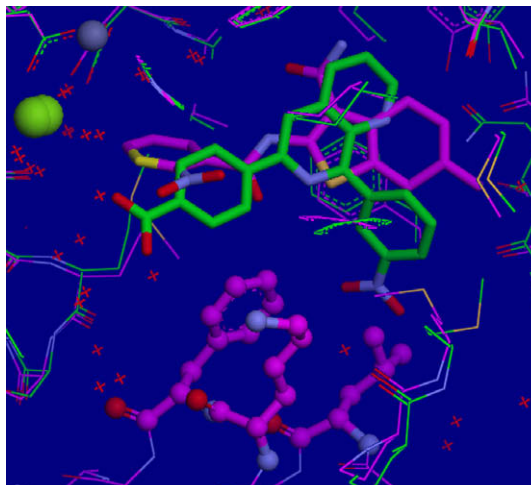
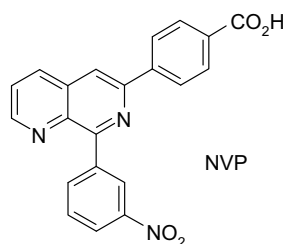


Figure 7. Overlay of PDE4B/THBT (magenta) and PDE4B/NVP (2qyl, 1.95 Å resol.; green) X-ray structures; three C-terminal side chains in ball and stick.

An alternative ligand-anchoring H bond is found between the primary ligand amide and Asn-395 as well as a water molecule at the back of the binding pocket (Fig. 4). Whereas the part of the ligand close to the metals stays within the space commonly occupied by PDE4 inhibitors, the THBT extends several Ångströms beyond this space at the opposite end. The established SAR in the THBT series can now be rationalised with this docking mode. The 4- and 5-positions of the tetrahydrobenzo group are deeply buried in the protein pocket and inaccessible for substitution. It is position 6, which is responsible for the subtype selectivity (Table 2), that extends towards Hlx-15. The 6-ethyl group gives maximal PDE4B activity of the groups in Table 2 whereas larger and smaller substituents decrease activity. While the degree of protein deformation seems to correlate with the level of 4B activity and 4B/4D selectivity, the mechanistic connection is not clear.

Notably, the THBT is 6 Å removed from the C-terminal helix fragment 498–509 (Fig. 5). Three C-terminal residues point into the binding pocket, Leu502Gln (4B amino acid/4B2 numbering/4D amino acid) Lys505Lys and Phe506Phe (Fig. 6), but only one of them can potentially be exploited for subtype-selective ligand design. So a ligand like NVP that extends towards this residue pair Leu/Gln in the PDE4B/4D co-crystal structures, respectively (Fig. 7),¹⁸ could exhibit subtype selectivity if a differential interaction between ligand and Leu/Gln can be achieved.

Other catalytic domain residues differing between 4B and 4D, like Gln416Arg in helix-14 and Thr436Asn in the helix-15/16 loop are more than 14 Å distant from the ligand. The orientation of both is affected by the helix shift induced by the THBT but both face towards the solvent (Fig. 5). It is not clear how this PDE4B/4D sequence difference around the ligand binding site, the movement of helix-15 and the nature of the C-terminal residues extending into the binding pocket contribute to the subtype selectivity observed for some of the THBT ligands.

3. Conclusions

In summary, the SAR of a 10-fold PDE4B-selective tetrahydrothiophene inhibitor series did not agree with either of two proposed docking modes derived from existing co-crystal structures for other PDE4 inhibitor templates. Eventually, the PDE4 co-crystal structure of a lead molecule was solved and surprised us twofold, with a considerable shift of the helix-15 backbone as well as the displacement of a crucial residue for ligand coordination (Gln-443). The unexpected binding mode emphasises the possibility of an induced fit effect even in a protein like the PDE4 catalytic

domain which has been rigid in dozens of previous apo and co-crystal structures.

4. Experimental

4.1. General

HPLC chromatography was performed using column: 3.3 cm × 4.6 mm ID, 3 μm ABZ + PLUS with a flow rate: 3 ml/min and injection volume of 5 μl at room temperature which was coupled to a UV detector with a range of 215–330 nm. Mass directed auto preparative chromatography was carried out using a Supelcosil ABZ+Plus column; 100 mm × 21.2 mm ID with a stationary phase particle size of 5 μm. ¹H NMR data were collected using the Bruker 400 MHz spectrometer using deuterated solvents and (CH₃)₄Si as the internal standard.

4.1.1. General procedure for the synthesis of n-substituted tetrahydrobenzothiophenes scaffolds

The cyclohexanone (1 equiv) 2-cyanoacetamide (1.05 equiv) and sulfur (1.05 equiv) were added to ethanol (6 ml/g) and heated to reflux. Morpholine (1.05 equiv) was added dropwise to the heating solution and the mixture was allowed to heat to reflux for 2–4 h. Upon cooling, a precipitate formed which was filtered and washed with cold ethanol. The precipitate was recrystallised from hot ethanol, filtered and dried to give the desired compound.

4.1.2. 2-Amino-6-methyl-4,5,6,7-tetrahydro-1-benzothiophene-3-carboxamide (11, where R1 = CH₃, R2 = R3 = H₂)

Orange solid (2.9 g, 51%); ¹H NMR (400 MHz, CDCl₃) δ 01.07 (d, J = 8 Hz, 3H), δ 1.42–1.48 (m, 1H), δ 1.89–1.94 (m, 2H), δ 2.16–2.23 (m, 1H), δ 2.57–2.63 (m, 2H), δ 2.74–2.78 (m, 1H), δ 5.40 (brs, 2H), δ 6.15 (brs, 2H); MS (ESI) m/z 211.13 (M+H)⁺; LC (eluent: acetonitrile/water, 0–100% gradient over 5 min); t 2.77 min.

4.1.3. 6-Methyl-2-[(2-nitrophenyl)carbonylamino]-4,5,6,7-tetrahydro-1-benzothiophene-3-carboxamide (6)

To a solution of the amine 7 (100 mg, 0.47 mmol) in pyridine (1 ml) was added 2-nitrobenzoyl chloride (1.2 equiv 0.57 mmol, 106 mg) and the reaction mixture allowed to stir at room temperature for 16 h. Upon completion, the reaction mixture was concentrated under vacuum and the crude mixture crystallised from hot ethanol to afford the desired compound (110 mg, 65%). ¹H NMR (400 MHz, CDCl₃) δ 01.12 (d, J = 8 Hz, 3H), δ 1.49–1.52 (m, 1H), δ

1.96–2.01 (m, 2H), δ 2.35–2.39 (m, 1H), δ 2.71–2.75 (m, 1H), δ 2.81–2.88 (m, 2H), δ 5.72 (br s, 2H), δ 7.63–7.74 (m, 3H), δ 8.06–8.08 (d, J = 8 Hz, 1H) δ 12.62 (s, 1H); MS (ESI) m/z 360.23 (M+H)⁺, 358.28 (M–H)⁺; LC (eluent: acetonitrile/water, 0–100% gradient over 5 min); t 3.31 min.

Compounds in Tables 1 and 2. From 11, the general procedure described for the synthesis of 6 was followed.

5. Crystallography

The PDE4B2B (residues 152–528, triple mutant [S482A, S487A, S489A]) was expressed in Baculovirus infected Sf9 cells and purified as described previously.¹⁹ To minimise C-terminal cleavage (to 503) during cell breakage and extraction, a protease inhibitor cocktail was included (Roche complete tablets). After clarification by centrifugation and filtration, PDE4B2 protein was purified on Q-Sepharose FF and Cibacron Blue Sepharose FF. The eluate was applied to a 10 ml Q-Sepharose HP column and eluted with a NaCl gradient to separate out any cleaved protein. Intact protein was further purified by size exclusion on a Superdex 200 column (26/60) and finally dialysed into 10 mM Hepes, pH 7.0, 20 mM NaCl, 0.1 mM EDTA for crystallography. Purified protein was concentrated to 16–20 mg/ml in 10 mM Hepes, pH 7.0, 20 mM NaCl, 0.1 mM EDTA, 5 mM DTT.

X-ray quality co-crystallisation was set up as a hanging drop experiment at 4 °C using 1 μ l + 1 μ l drops with protein (with sixfold molar excess of inhibitor) and a well solution containing 18% PEG 4000, 18% glycerol, 0.08 M MES pH 6.8, 0.45 M NaCl, 0.15 M MgCl₂, 0.05 M Na acetate, 0.05 M Mg acetate and 0.025 M ammonium sulfate. The crystals reached full size within four weeks.

X-ray diffraction data were collected to 2.23 Å resolution at the ESRF (station ID23.1) using a ADSC Q315 CCD detector and processed as space group $P4_1$ with MOSFLM²⁰ and SCALA within the CCP4 programme suite.²¹ The structure was solved by Molecular Replacement using PHASER²² and a search model derived from 1FOJ. Refinement was performed using REFMAC²³ to a final R -factor = 17.9% (R -free = 22.9%). The coordinates consisted of two molecules in the asymmetric unit, each with a bound inhibitor. All residues were built (in both molecules) except 486–494 and 512–528 that were too disordered. The coordinates have been deposited in the PDB as deposition code 3HMV.

Acknowledgements

We would like to thank Surjit Bains, Girish Shah and Phil Hardwick for protein expression and Martin Fillmore for early chemistry development. GlaxoSmithKline funded this work.

References and notes

- Cheung, W. Y. *Biochemistry* **1967**, *6*, 1079.
- Schwabe, U.; Miyake, M.; Ohga, Y.; Daly, J. *Mol. Pharmacol.* **1976**, *12*, 900.
- Dastidar, S. G.; Rajagopal, D.; Ray, A. *Curr. Opin. Invest. Drugs* **2007**, *85*, 364.
- Jin, S.-L. C.; Lan, L.; Zoudilova, M.; Conti, M. J. *Immun.* **2005**, *175*, 1523.
- Robichaud, A.; Stamatou, P. B.; Jin, S.-L. C.; Lachance, N.; MacDonald, D.; Laliberte, F.; Liu, S.; Huang, Z.; Conti, M.; Chan, C.-C. *J. Clin. Invest.* **2002**, *110*, 1045.
- Zhang, K. Y. J.; Card, G. L.; Suzuki, Y.; Artis, D. R.; Fong, D.; Gillette, S.; Hsieh, D.; Neiman, J.; West, B. L.; Zhang, C.; Milburn, M. V.; Kim, S.-H.; Schlessinger, J.; Bollag, G. *Mol. Cell* **2004**, *15*, 279.
- Inhibition of PDE4B and PDE4D were measured using a luminescence-coupled assay system developed by Cambrex. This assay system couples the formation of AMP, derived from PDE4-catalyzed hydrolysis of cAMP, to the formation of ATP. The ATP is then used as a substrate for Luciferase and results in light as a signal output. When PDE is inhibited or inactive, no AMP is produced, the luciferase is inactive, and no light signal is produced. This assay is used in a quenched assay format, where PDE4 enzyme (2.5 μ l; ~120 pM enzyme in 40 mM Tris-HCl, 10 mM MgCl₂, 1 mM CHAPS, 0.01% BSA, pH 7.5.) and cAMP substrate (2.5 μ l; 2 μ M cAMP in 40 mM Tris-HCl, 10 mM MgCl₂, 1 mM CHAPS, 0.01% BSA, pH 7.5.) are added sequentially to a 384 well assay plate (Greiner 784075) pre-stamped with 12.5–50 nL compound at the desired concentration. The reaction is incubated at room temperature for 1 h, then is quenched by the addition of enzyme stop solution (1.5 μ l; prepared as described by vendor; catalog # LT27-253) and then the light signal is generated by the addition of detection reagent (2.5 μ l, prepared as described by vendor, catalog# LT27-250). The luminescence is then measured on a Viewlux imager (Perkin Elmer) using emission filters of 613/55 nm or 618/40 nm and a 5 s. Compounds are prepared in neat DMSO at a concentration of 10 mM. For inhibition curves, compounds were diluted using a three fold serial dilution and tested at 11 concentrations (e.g., 50 μ M–0.8 nM or 25 μ M–0.42 nM or 2.5 μ M–42 pM). Curves were analysed as describe above using ActivityBase and Xlfit, and results were expressed as pIC_{50} values. Average standard deviations are for PDE4B = 0.10 and PDE4D = 0.11.
- Allen, F. H. *Acta Crystallogr., Sect. B* **2002**, *58*, 380.
- Lee, M. E.; Markowitz, J.; Lee, J.-O.; Lee, H. *FEBS Lett.* **2002**, *530*, 53.
- Allen, F. H.; Bird, C. M.; Rowland, R. S.; Raithby, P. R. *Acta Crystallogr. Sect. B* **1997**, *53*, 696.
- McMartin, C.; Bohacek, R. S. *J. Comp. Aided Mol. Des.* **1997**, *11*, 333.
- Card, G. L.; England, B. P.; Suzuki, Y.; Fong, D.; Powell, B.; Lee, B.; Luu, C.; Tabrizizad, M.; Gillette, S.; Ibrahim, P. N.; Artis, D. R.; Bollag, G.; Milburn, M. V.; Kim, S.-H.; Schlessinger, J.; Zhang, K. Y. J. *Structure* **2004**, *12*, 2233.
- Gewald, K.; Schael, J. *J. Prakt. Chem.* **1973**, *315*, 39.
- Houslay, M. D.; Adams, D. R. *Biochem. J.* **2003**, *370*, 1.
- McLaughlin, M. M.; Cieslinski, L. B.; Burman, M.; Torphy, T. J.; Livi, G. P. *J. Biol. Chem.* **1993**, *268*, 6470.
- Xu, R. X.; Hassell, A. M.; Vanderwall, D.; Lambert, M. H.; Holmes, W. D.; Luther, M. A.; Rocque, W. J.; Milburn, M. V.; Zhao, Y.; Ke, H.; Nolte, R. T. *Science* **2000**, *288*, 1822.
- Manuscript in preparation.
- Wang, H.; Peng, M.-S.; Chen, Y.; Robinson, H.; Houslay, M. D.; Cai, J.; Ke, H. *Biochem. J.* **2007**, *408*, 193.
- Rocque, W. J.; Holmes, W. D.; Patel, I. R.; Dougherty, R. W.; Ittoop, O.; Overton, L.; Hoffman, C. R.; Wisely, G. B.; Willard, D. H.; Luther, M. A. *Protein Exp. Purif.* **1997**, *9*, 191.
- Leslie, A. G. W., Joint CCP4+ESF-EAMCB Newsletter on Protein Crystallography, 1992, No. 26.
- Bailey, S. *Acta Crystallogr. Sect. D* **1994**, *50*, 760.
- Storoni, L. C.; McCoy, A. J.; Read, R. J. *Acta Crystallogr. Sect. D* **2004**, *60*, 432.
- Murshudov, G. N.; Vagin, A. A.; Dodson, E. J. *Acta Crystallogr. Sect. D* **1997**, *53*, 240.